



Original Research Article

A Novel Approach in the Synthesis of Indoloquinoline Alkaloid Analogues: Spectroscopic and DFT Exploration, Molecular Docking of COVID-19 and ADMET Properties

M. Vijayarathinam , A. Kannan * , P. Akilan , V. Chandrasekaran, T. Gunasekaran

Department of Chemistry, Government Arts College (Autonomous), Affiliated to Periyar University, Salem, Tamil Nadu, India, 636007

ARTICLE INFO

Article history

Submitted: 17 January 2024

Revised: 16 February 2024

Accepted: 27 March 2024

Manuscript ID: [AJCA-2401-1484](https://doi.org/10.48309/AJCA.2024.437859.1484)

Checked for Plagiarism: Yes

Language Editor Checked: Yes

DOI: [10.48309/AJCA.2024.437859.1484](https://doi.org/10.48309/AJCA.2024.437859.1484)

KEYWORDS

Claisen condensation

Indoloquinoline

In-silico molecular docking

COVID-19

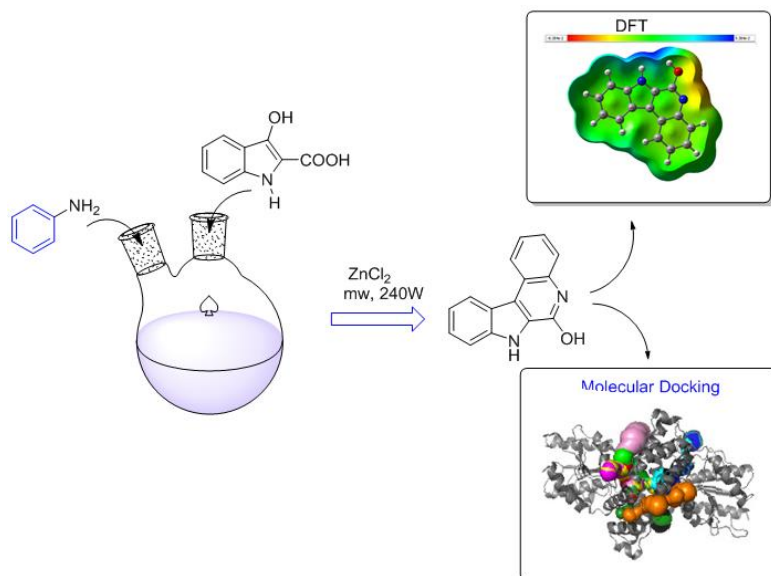
DFT

ADMET analysis

ABSTRACT

A succinct total synthesis of an indoloquinoline alkaloid was achieved through a one-pot, two-step process involving a cascade of sodium hydride and aniline, followed by a base-mediated Claisen condensation reaction. Subsequently, the reaction was conducted *via* microwave-assisted synthesis (MAS), resulting in a good yield of the title compound with eco-friendly methodologies. The structural properties of the synthesized compound were validated using FT-IR, ¹H-NMR, ¹³C-NMR, and GC-Mass spectral analyses. In addition, FT-IR approaches were employed to compare the vibrational wavenumbers obtained through simulation with experimental wave numbers. Furthermore, DFT calculations were employed to fine-tune the structural parameters and investigate FMOs, Mulliken atomic charges, MEP, and NLO properties, and molecular docking studies evaluated its N₃ binding site of the primary coronavirus protein 6LU7. Likewise, the title compound is assessed for its ADMET (Absorption, Distribution, Metabolism, Excretion, and Toxicity) properties, revealing promising pharmacokinetic profiles devoid of any detected indications of non-toxicity.

GRAPHICAL ABSTRACT



* Corresponding author: Kannan, A.

✉ E-mail: ch.vram@yahoo.in

© 2024 by SPC (Sami Publishing Company)

Introduction

The indoloquinoline alkaloids, which have a quinoline and indole fused system, are important [1-3]. Notable members of this class include the linear indoloquinoline alkaloid cryptolepine (1) [4,5], cryptotackieine (2), nor-cryptotackieine (3), and the angularly fused alkaloid cryptosanguinolentine (4). In addition, isonecryptolepine (5) was also classified within this group (Figure 1) [6-8]. Isoncryptolepine alkaloid is derived from a plant of *Cryptolepis sanguinolenta*. Given its designation, isonecryptolepine also has antiplasmodial properties and shares several biological characteristics [9]. These include antimicrobial effects, cytotoxicity and DNA intercalation [9]. Cryptolepine and iso-cryptolepine have a traditional application in addressing a wide range of health issues, being employed in clinical therapy for conditions including rheumatism, urinary tract infections of anti-bacterial [11], and malaria diseases [12-14]. The characterization of the designated compound involved the optimization of its structure using DFT at the B3LYP/6.311G* method, focusing on 7H-indolo[2,3-c]quinolinol (IQOL). Subsequently, theoretical investigations into the compound's reactivity were carried out. The investigation integrated both experimental and DFT approaches for FT-IR [15-20].

The synthesis and analysis of indolequinone moieties have been undertaken due to their anti-coronavirus-19 (COVID-19) properties [19], employing computational methodologies to expedite.

The identification and development of innovative therapeutic drug molecules. This method utilizes computational approaches and initial insights from SAR investigations. The results of these studies indicate that optimization may be achieved through precise adjustments to the nature of the substituents on indoloquinoline derivatives [22-24]. Assessing the ADME-Tox analysis of a drug molecule is crucial for researching new drug formulations [25-27].

Recently, chloroquine and hydroxychloroquine have gained prominence as significant medical treatments for COVID-19, ranking among the most prescribed medications in the USA, with more than ten million recommendations. Quinoline alkaloids, a category of compounds used in treating malaria fever infection, have shown efficacy in inhibiting viral replication in diverse infections, including those induced by the SARS-associated coronavirus (CoV) and MERS-CoV. The quinoline heterocyclic structure has proven to be a robust approach in medicinal chemistry research. The exploration of organic synthesis through one-pot, tandem Claisen research in organic chemistry, notably propelling

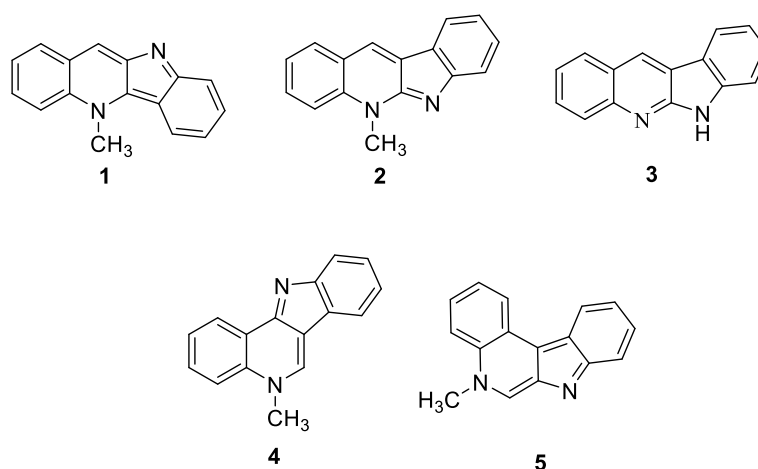


Figure 1. Some selective family of indoloquinoline alkaloids.

drug discovery initiatives. The Claisen condensation reaction is a classical and valuable multicomponent reaction that facilitates the assembly of pharmacologically active quinoline and indole derivatives from commercially available precursors. This advancement holds promise for accelerating drug discovery programs in the field of organic chemistry [28,29].

We devised and synthesized the drug discovery (IQOL), capable of systematically studying and completing the synthesis of a distinctive compound using computer-generated tools. IQOL has effective inhibitory effects on COVID-19. Furthermore, *in silico* molecular docking analysis were conducted with the main protein structures of covid-19 (PDB: 6LU7) [29,30]. The approach employed a structure-assisted drug design [32,33]. The primary focus of this program was to pinpoint drug leads targeting the SARS-CoV-2 protein. Finally, ADME/Tox studies [34–37] and [38].

Experimental

Synthesis of 3-hydroxyindole-2-carboxylic acid

Scheme 1 by employing two different routes. In Route A, an equimolar mixture of 1-chlorobenzoic acid 1 (1.57 g, 0.01 mol) and glycine 2 (0.76 g, 0.1 mol), along with (0.50 g) of sodium hydride was added. The resultant mixture underwent microwave radiation at 240 W for 10 minutes.

For Route B, an 0.01 equimolar mixture of ethyl bromoacetate 3 (1.65 g) and methylanthranate (1.6 mL), along with (0.50 g) of sodium hydride, was employed, and then the reaction mixture at 240 W in a microwave oven, 5-10 minutes, The completion of the reaction was confirmed through TLC. It was subsequently purified through column chromatography. The final step included recrystallization from ethanol, leading to a satisfactory 71% yield of the desired product.

FT-IR (KBr, ν_{\max} , cm^{-1}): (Figure S1) 3444, 3389, 3048, 1702, 1603, 1445, 1356; 1299, 1188, 881, and 740. $^1\text{H-NMR}$ (400 MHz, DMSO- d_6): (Figure S2) δ 12.94 (bs, 10H, C₂-COOH), 12.78 (s, H, N-H), 7.96 (dd, $J = 8.0$, indole - C₄H and HC₇), 7.62 (t, indole HC₆), and 7.50 (t, HC₅), $^{13}\text{C-NMR}$ (100 MHz, DMSO- d_6) (Figure S3) $\delta = 167.79, 133.30, 133.03, 131.24, 129.94, 129.72, 129.52, 129.18, 129.01$. HRMS (ESI, m/z), (Figure S4) C₉H₇NO₃ [M+H]. = 177.68.

Preparation of IQOL

The mixture comprising equimolar quantities of 3-hydroxyindole-2-carboxylic acid 5 (17.7 g, 0.1 mol) and aniline (9.0 mL, 0.1 mol), along with (0.50 g) of ZnCl₂, was introduced [39]. The reaction proceeded under microwave oven conditions at 250 W (180 °C) for 10-15 minutes. A yellow solid was produced, the validity of the reaction procedure was verified through TLC. When the reaction mixture attained room temperature, it was transferred to 500 mL of ice water and neutralized. The formed solid precipitate was filtered, subsequently purified through column chromatography, and subjected to recrystallization from ethanol. resulting in the formation of a yellow solid 63% yield.

FT-IR (KBr, ν_{\max} , cm^{-1}): (Figure S5) 3487, 3319, 3129, 3073, 1675, 1594, 1496, 1291, 1182, 816, and 754. $^1\text{H NMR}$ (400 MHz, DMSO- d_6): (Figure S6) δ 16.22 (bs, OH), 11.52 (s, 1H-N), 7.87 (d, $J = 8.4$, indole HC₁₁), 7.54 (dd, $J = 8.0$, quinoline C₅-H), 7.50-7.41 (q, C₂-H and C₈-H), 7.30 (t, H C₃), 7.10 (t, HC₄), 7.05 (t, 1H, HC₉), and 6.89 (t, 1H, HC₁₀). $^{13}\text{C-NMR}$ (100 MHz, DMSO- d_6) (Figure S7) $\delta = 162.51, 157.51, 139.05, 138.09, 137.61, 133.60, 132.69, 129.53, 129.33, 128.58, 127.82, 125.99, 125.76, 125.43, 122.01, 121.43, 120.49, 119.82, 111.75, 109.98, \text{ and } 106.74$; HRMS (ESI, m/z) (Figure S8); C₁₅H₁₀N₂O [M-H]. = 233.33.

DFT controls

Quantum mechanism simulations were carried out with the Gauss view and Gaussian 09 W programme. Becke's three-parameter hybrid exchange-correlation functional (B3LYP) with a 6-311G (d,p) basis set was used for these computations. Energy assessment and IR spectra calculation involved performing frequency calculations using the cam B3LYP/6-311+G(d) level of the DFT method.

In addition, FT-IR calculations at the same wave number computation level were conducted. Root mean square (RMS) errors were calculated for both FT-IR methods. The optimized structure was used to calculate the geometry parameters, FMOs- frontier molecular orbitals, global electronic properties study, and molecular electrostatic potential (MEP) of the compound IQOL. For energy evaluation and IR spectral computation, FT-IR studies were undertaken using the same wave-number computation level. Furthermore, our analysis involved simulating wavenumbers in Fourier transform infrared (FT-IR).

The Gauss-Sum software program was used to generate a density of states (DOS) plot, Global electronic properties such as HOMO and LUMO, energy gap (ΔE), electronegativity (χ), and reactivity indices, including electronic chemical potential (μ), chemical hardness (η), softness (σ), ionization potential (I), electron charge transfer (ΔN), global electrophilicity (ω), and global nucleophilicity (N), were computed using the following expressions: $\mu = (E_{\text{HOMO}} + E_{\text{LUMO}})/2$, $\eta = (E_{\text{LUMO}} - E_{\text{HOMO}})$, $\omega = \mu^2/2\eta$, and $N = E_{\text{H}} - E_{\text{H}}(\text{TCE})$ [40,41].

Molecular docking

Structure-based drug design often involves molecular docking analysis. In this process, the designed ligand synthesized IQOL was visualized, The energy-minimized ligand (structures) Chemoffice (Cambridge Software) in SDF formats

were converted to mol2 files using open babel and the COVID-19 protein 6lu7 as downloaded from (<http://www.pdb.org>) website of pdb type format, further hydrogen and water molecules. The docking was conducted using the AutoDock Vina Wizard method.

The parameters for the VINA grid box size (X= -10.7290, Y = 12.4176, and Z = 68.8161) were adjusted, Use the standard exhaustiveness level of 8 to improve the binding conformation evaluation. The visual representations of entirely docked structures were created with Discovery Studio -2021 and PyMOL program package.

Pharmacological/biological assays

ADME/Tox

ADME/Tox analyses utilized both the Swiss adme and protox software of predictor. contains critical computational approaches for fully evaluating the pharmacokinetic characteristics of tiny compounds.

Results and Discussion

Chemistry

The current study, indoloquinoline alkaloid (IQOL), as shown in Scheme 1, found convincing support from ^1H and ^{13}C -NMR, FT-IR, and GC-Mass spectrums. Notably, the remaining structures only showed signals for IQOL, indicating the importance of N-H and hydroxy groups interactions of drug targets.

Synthetic routes for the desired indoloquinoline derivatives. The two-step transformation of IQOL involves an initial synthesis of 3-hydroxy-1H-indole-2-carboxylic acid **5** through two distinct routes.

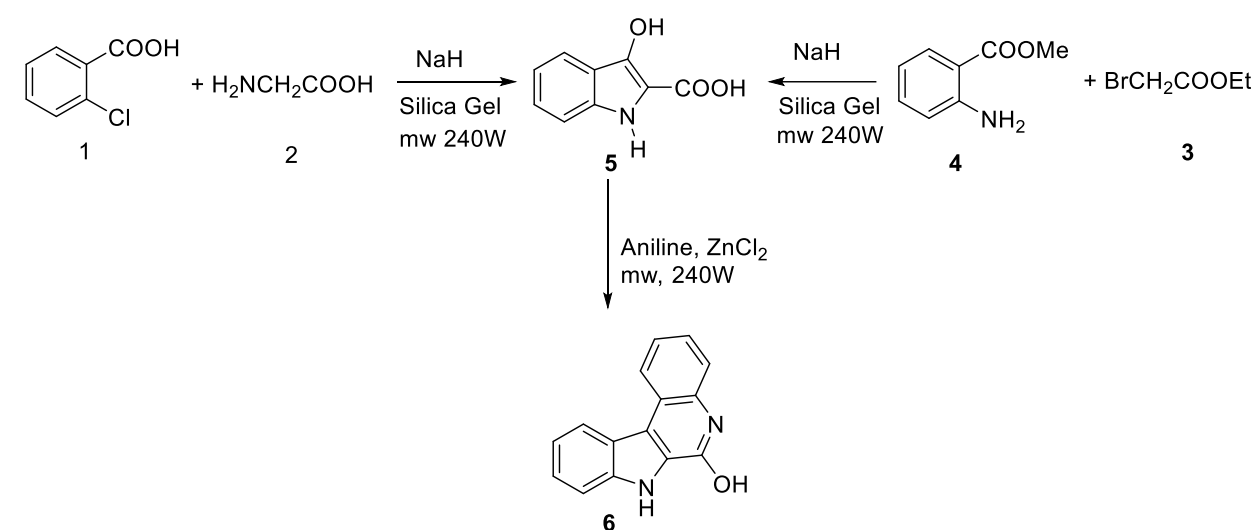
Route A utilizes 1-chlorobenzoic acid **1** with glycine **2**, while Route B employs ethyl bromoacetate **3** with methylanthranate **4**. The subsequent step involved the reaction of 3-hydroxy-1H-indole-2-carboxylic acid **5** with

aniline to produce the title compound. This procedure involves thermally induced intramolecular cyclization carried out at an elevated temperature (240 °C) under solvent-free conditions.

The suggested strategy uses the Claisen reaction technology, which involves cyclization with the help of sodium hydride. Despite the anticipation of the formation of IQOL (6), it was still present.

A possible strategy for the formation of IQOL involves employing the Claisen ester condensation mechanism, facilitated by the use of sodium hydride as a robust reagent under mediated conditions

Spectral analysis of IQOL



Scheme 1. Route for synthesis of indoloquinoline alkaloid analogues.

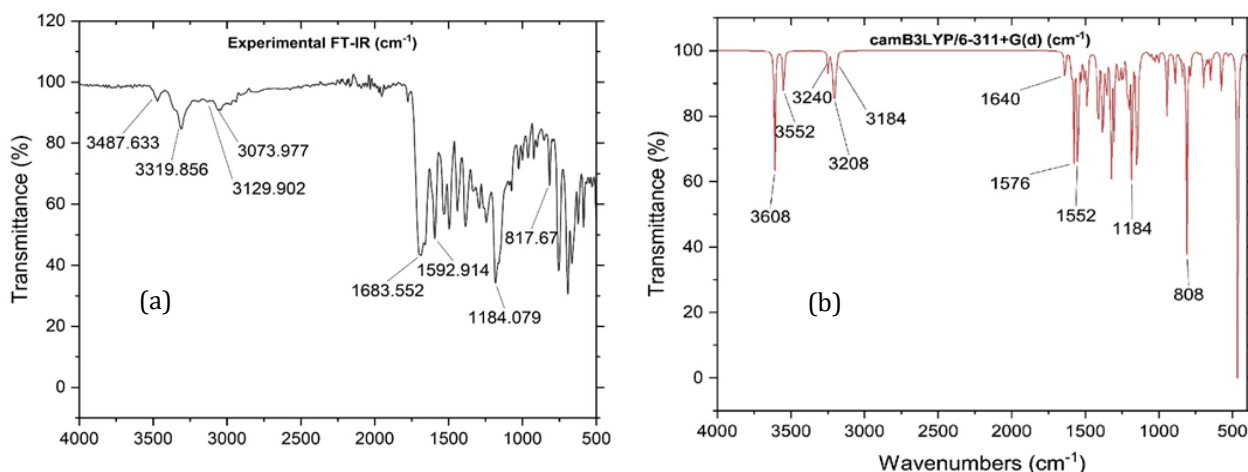


Figure 2. FT-IR spectra of IQOL (a) experimental and (b) calculated.

FT-IR spectral analysis

The molecular structure under discussion is an IQOL with 28 atoms, C1 point group plane symmetry, and 78 normal vibrational modes. These modes include 27 stretching, 26 bending, and 25 torsional vibrations. DFT FT-IR was obtained using B3LYP/6.311+G (d,p) parameter calculations, and then compared to experimental data. Results are shown in [Table 1](#) and [Figure 2](#).

CH frequency

Normally, CH stretching mode of aromatic rings is not significantly affected by substituent groups. However, specific vibrations can penetrate to substituents, providing respected structural visions toward their mechanical coupling through substituent group vibration. The 3100-3000 cm^{-1} asymmetric stretching is observed. While symmetric stretches at 3000-2900 cm^{-1} region.

In the ongoing analysis of the title compound IQOL, experimental observations indicated the existence of aromatic C-H asymmetric stretching 3129 cm^{-1} . The theoretic peak of the FTIR appeared at 3208 cm^{-1} . Experiments revealed symmetric $\nu(\text{C-H})$ vibrations. identified at 3073 cm^{-1} with weak absorption peaks, while the calculated frequency was 3184 cm^{-1} . Comparable results were experimentally confirmed and are illustrated in [Figure 2](#) and [Table 1](#)

C-N frequency

Assigning the stretching of C-N frequency usually found in the range of 1650-1500 cm^{-1} . Experimental profiles corresponding to the C-N frequency showed significant and conspicuous peaks at 1592 and 1291 cm^{-1} , while the computational calculations gave values of 1576 and 1293 cm^{-1} , respectively.

C-C frequency

The stretching vibrations of C=C bonds are spectral range of 1650-1300 cm^{-1} . Experimental vibrations were identified at 1496, 1385, 1291, and 933 cm^{-1} , with DFT computed vibration values are closely matching 1479, 1382, 1293, and 932 cm^{-1} , correspondingly, and experimental region of C-C stretching vibrational frequency was noted at 1074 and 1182 cm^{-1} , aligning well with the matching DFT computed vibrations detected at 1087 and 1184 cm^{-1} .

N-H frequency

Indoloquinoline ring N-H group stretching mode of frequencies, detected at 3319 cm^{-1} experimentally, exhibit notable concordance with the DFT calculated slow at 3551 cm^{-1} .

OH frequency

The OH stretching vibrational typically ensues in the increased spectral values resulting from the electronegativity of the bond between oxygen and hydrogen atoms (OH). Affording to the literature, the reported wavenumber for the OH band is within the range of 3350-3600 cm^{-1} . Still, in certain instances, the OH frequency may increase after the OH group is involved in either inter-intra molecular hydrogen bonding. the OH stretching frequency was detected at 3487 cm^{-1} experimentally, with a corresponding theoretical measurement at 3608 cm^{-1} .

NMR spectral data analysis

$^1\text{H-NMR}$ spectrum; a broad singlet for one proton is observed in the downfield region, at δ 11.52 ppm, designated as the indole-N-H proton. In addition, a broad singlet is identified in the downfield region above 15.00 ppm, assigned to the hydroxy group of the quinoline moiety.

Table 1. DFT computed and experimental FT-IR spectra of IQOL

Functional group	camB3LYP/6-311+G(d) (cm ⁻¹)	Experimental (cm ⁻¹)
O-H	3608	3487
N-H	3551	3319
C-N	1576, 1293	1592, 1291
C-C	1087, 1182	1074, 1182
C-H Aromatic	3208, 3184	3129, 3073

The aromatic region displays proton signals in the downfield from δ 6.89 to 7.88, encompassing eight proton integral values corresponding to the indoloquinoline moiety, as illustrated in Figure S2.

The pertinent ¹³C-NMR spectrum is illustrated in Figure S3, revealing a less intense peak at 162.51 ppm, which was assigned unequivocally to the C₆-OH carbon and corresponded to the hydroxy group attached to quinoline. Another less intense peak at 157.51 ppm is observed in the most downfield region, suggestive of the C₇-N group carbon signal, confirming IQOL formation. This is further supported by the observation of aromatic carbon signals for (IQOL) in the range of 154.94 to 106.74 ppm.

Furthermore, the suggested structure was confirmed through the GC-MS spectrum (Figure S4), where a (m/z) at 233.33 (observed) closely concurred with the calculated molecular mass

(234). The [M-1] fragmentation peak, which accounts for 99% appeared parent peak matches perfectly the mass value of compound and is consistent with the formula for the suggested [C₁₅H₁₀N₂O]. Further support confirmed the GC-mass spectra of title compound IQOL.

DFT analysis

Optimization of IQOL

The structure of the IQOL molecule was optimized by utilizing density functional theory at the B3LYP level of computation. This approach was used to improve the geometrical characteristics of bond lengths, angles, and dihedral angles in the IQOL. The geometrical characteristics show that the indoloquinoline ring has a planar structure. The optimized geometric structure is shown in Figure 3 and Table 2.

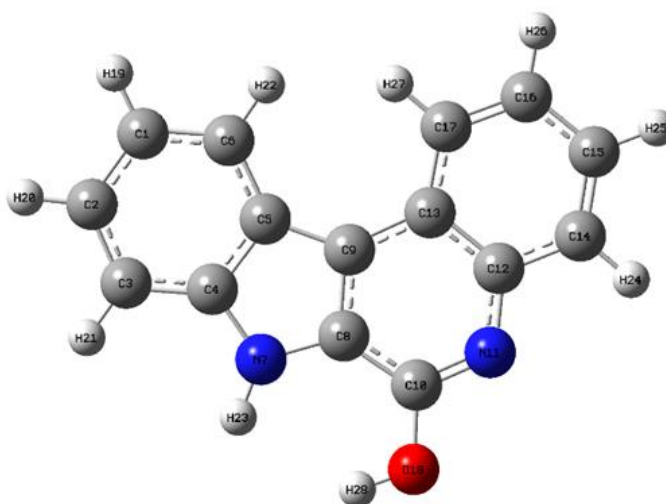
**Figure 3.** Optimized structure of IQOL.

Table 2. The bonds and their parameters of IQOL

Atoms	DFT Bond Lengths (Å)	Atoms	DFT Bond Lengths (Å)
R(1,2)	1.4094	R(8,10)	1.423
R(1,6)	1.3906	R(9,13)	1.4317
R(1,19)	1.0856	R(10,11)	1.2993
R(2,3)	1.391	R(10,18)	1.3691
R(4,5)	1.4234	R(13,17)	1.4163
R(4,7)	1.3844	R(14,15)	1.3812
R(5,6)	1.4075	R(14,24)	1.0853
R(5,9)	1.4503	R(15,16)	1.4119
R(6,22)	1.0835	R(15,25)	1.0861
R(7,8)	1.389	R(16,17)	1.383
R(7,23)	1.0071	R(16,26)	1.0861
R(8,9)	1.4016	R(17,27)	1.0835
		R(18,28)	0.9646
A(2,1,6)	121.0758	A(5,9,13)	135.0228
A(2,1,19)	119.3815	A(8,9,13)	118.5149
A(6,1,19)	119.5427	A(8,10,11)	121.8969
A(1,2,3)	121.0595	A(8,10,18)	122.2318
A(1,2,20)	119.5233	A(11,10,18)	115.8713
A(3,2,20)	119.4172	A(10,11,12)	119.7286
A(2,3,4)	117.5559	A(11,12,13)	123.3381
A(2,3,21)	121.1305	A(11,12,14)	117.4782
A(4,3,21)	121.3136	A(13,12,14)	119.1837
A(3,4,5)	122.6053	A(9,13,12)	116.0737
A(3,4,7)	128.8908	A(9,13,17)	125.2836
A(5,4,7)	108.5039	A(12,13,17)	118.6427
A(4,5,6)	118.2909	A(12,14,15)	120.795
A(4,5,9)	106.6533	A(12,14,24)	117.5638
A(6,5,9)	135.0558	A(15,14,24)	121.6412
A(1,6,5)	119.4127	A(14,15,16)	120.1132
A(1,6,22)	119.5589	A(14,15,25)	120.0464
A(5,6,22)	121.0284	A(16,15,25)	119.8403
A(4,7,8)	108.8301	A(15,16,17)	120.3804
A(4,7,23)	123.9325	A(15,16,26)	119.8756
A(8,7,23)	127.2374	A(17,16,26)	119.744
A(7,8,9)	109.5504	A(13,17,16)	120.8849
A(7,8,10)	130.0017	A(13,17,27)	119.7276
A(9,8,10)	120.4479	A(16,17,27)	119.3875
A(5,9,8)	106.4623	A(10,18,28)	111.49

Table 2. Continued...

Atoms	DFT Dihedral Angles (°)	Atoms	DFT Dihedral Angles (°)
D(6,1,2,3)	0.0003	D(10,8,9,13)	0.0026
D(6,1,2,20)	-180	D(7,8,10,11)	179.9989
D(19,1,2,3)	-180	D(7,8,10,18)	0
D(19,1,2,20)	0.0001	D(9,8,10,11)	-0.003
D(2,1,6,5)	-0.0001	D(9,8,10,18)	179.998
D(2,1,6,22)	180	D(5,9,13,12)	-179.999
D(19,1,6,5)	-180	D(5,9,13,17)	0.0001
D(19,1,6,22)	0	D(8,9,13,12)	-0.0005
D(1,2,3,4)	0	D(8,9,13,17)	179.9987
D(1,2,3,21)	179.9997	D(8,10,11,12)	0.0011
D(20,2,3,4)	-180	D(18,10,11,12)	180.0001
D(20,2,3,21)	-0.0001	D(8,10,18,28)	-0.0242
D(2,3,4,5)	-0.0006	D(11,10,18,28)	179.9768
D(2,3,4,7)	179.9997	D(10,11,12,13)	0.0011
D(21,3,4,5)	179.9997	D(10,11,12,14)	-180
D(21,3,4,7)	0	D(11,12,13,9)	-0.0014
D(3,4,5,6)	0.0008	D(11,12,13,17)	179.9994
D(3,4,5,9)	-179.999	D(14,12,13,9)	179.9992
D(7,4,5,6)	-179.999	D(14,12,13,17)	0
D(7,4,5,9)	0.0006	D(11,12,14,15)	-179.999
D(3,4,7,8)	179.9991	D(11,12,14,24)	0.0006
D(3,4,7,23)	0.0072	D(13,12,14,15)	0
D(5,4,7,8)	-0.0007	D(13,12,14,24)	180
D(5,4,7,23)	-179.993	D(9,13,17,16)	-179.999
D(4,5,6,1)	-0.0004	D(9,13,17,27)	0.0004
D(4,5,6,22)	179.9995	D(12,13,17,16)	0.0001
D(9,5,6,1)	179.9995	D(12,13,17,27)	179.9996
D(9,5,6,22)	-0.0006	D(12,14,15,16)	0
D(4,5,9,8)	-0.0004	D(12,14,15,25)	180
D(4,5,9,13)	179.9983	D(24,14,15,16)	-180
D(6,5,9,8)	179.9997	D(24,14,15,25)	0
D(6,5,9,13)	-0.0016	D(14,15,16,17)	0
D(4,7,8,9)	0.0005	D(14,15,16,26)	-180
D(4,7,8,10)	179.9987	D(25,15,16,17)	-180
D(23,7,8,9)	179.992	D(25,15,16,26)	0.0002
D(23,7,8,10)	-0.0098	D(15,16,17,13)	0
D(7,8,9,5)	-0.0001	D(15,16,17,27)	-180
D(7,8,9,13)	-179.999	D(26,16,17,13)	179.9998
D(10,8,9,5)	-179.999	D(26,16,17,27)	0.0002

Mulliken atomic charge analysis

The analysis of Mulliken population is beneficial for approximating the charge distribution among atoms in a compound. Depending on the neighboring electrons, Mulliken charges are assigned as either positive or negative. In Figure

4 and Table 3 [40], two atoms of oxygen are negatively charged, whereas some atoms of carbon (C5, C9, C10, C12, and C13) are positively charged. In contrast, the hydroxy group connected to C possesses a negative charge. Furthermore, all atoms of hydrogen carry positive charges.

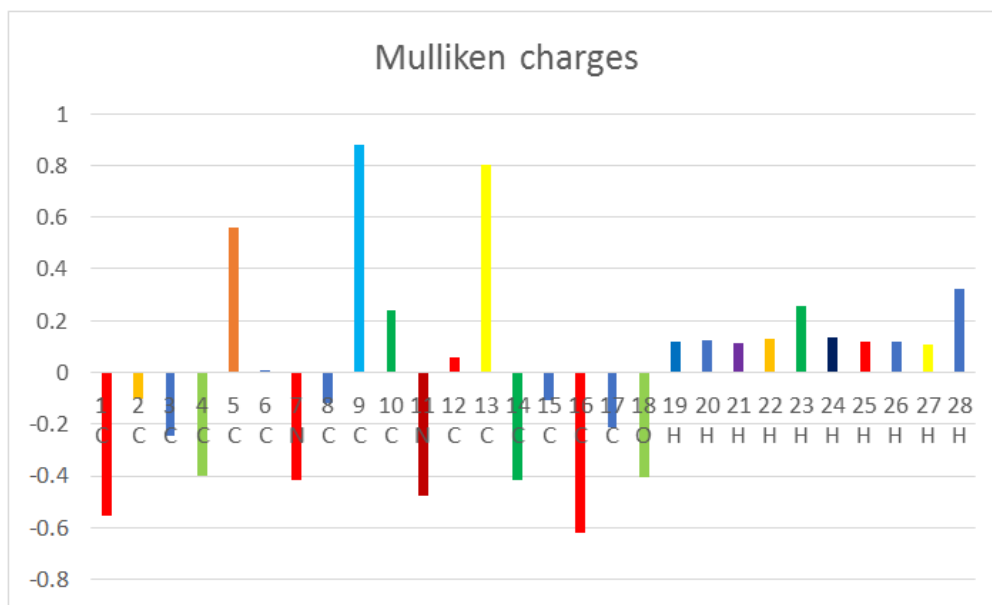


Figure 4. The Mulliken atomic charges of IQOL.

Table 3. The Mulliken atom charges of IQOL

Atom numbers	Charges	Atoms numbers	Charges
1 C	-0.1932	15 C	-0.10016
2 C	-0.22189	16 C	-0.50781
3 C	-0.61253	17 C	-0.0934
4 C	-0.62091	18 O	-0.40591
5 C	0.829327	19 H	0.126366
6 C	-0.20816	20 H	0.128726
7 N	-0.40878	21 H	0.11924
8 C	-0.57431	22 H	0.124577
9 C	1.165317	23 H	0.273995
10 C	0.604012	24 H	0.137516
11 N	-0.39324	25 H	0.125255
12 C	-0.30003	26 H	0.124651
13 C	0.57558	27 H	0.107174
14 C	-0.13495	28 H	0.333545

NLO

Dipole movement, polarizabilities / hyperpolarizabilities reveal how the system reacts to a specific field approach. These parameters characterize the system's nonlinear properties, including the cross-sectional areas of different scatter along with collision operations and the power of interactions between molecules. We determined the dipole moment (μ), hyperpolarizability (β), and polarizability (α) of the IQOL compound to study the association involving the structure of molecules and nonlinear capabilities. This contact increases the molecule's polarity and is useful for intramolecular relationships. A lower band energy gap is projected to result in improved NLO properties. The hydroxyquinoline ring, functioning as an electron donor in the IQOL

molecule, improves these delocalized electron densities associated with substitutes, resulting in organic NLO material properties.

The results, as outlined in Table 4, indicate values of $\alpha = 4.3313$ Debye, $\mu = -4.276256 \times 10^2$ e.s.u., and $\beta = 7.591340 \times 10^3$ e.s.u. for IQOL in contrast to urea as the benchmark [42]. As a result, we deduce that IQOL has outstanding NLO (Non-linear optical) properties.

Frontier orbitals calculations (FMOs)

Molecular reactivity assessed via frontier molecular orbital (FMO) investigation, with the HOMO and LUMO playing important roles in influencing the structure's chemical stability. Eg and numerous chemical reactivity descriptors, help to characterise molecular behaviour.

Table 4. The NLO analysis of IQOL

Parameters	Dipole moment	Debye
μ_x		4.3154
μ_y		0.3710
μ_z		0.0001
		4.3313×10-30 esu
Polarizability		
α_{xx}		-98.5972
α_{xy}		14.5591
α_{yy}		-94.8806
α_{xz}		0.0009
α_{yz}		-107.3342
α_{zz}		0.0008
α_0		-4.276256 ×10-30esu
Hyperpolarizability		
β_{xxx}		16.3033
β_{xxy}		-3.7048
β_{xyy}		0.0059
β_{yyy}		11.6504
β_{xxz}		-0.0014
β_{xyz}		-0.0031
β_{yyz}		0.0004
β_{xzz}		-1.8477
β_{yzz}		47.1166
β_{zzz}		13.1383
β_0		7.591340×10-30esu

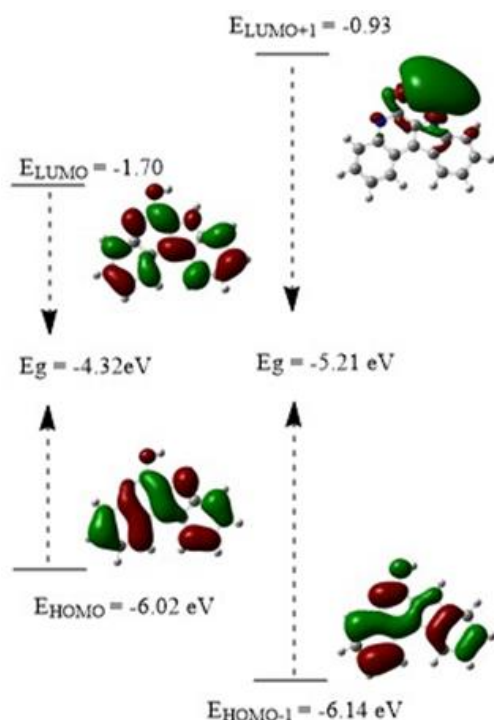


Figure 5. Energy levels of EHOMO, ELUMO, and Egap for the synthesized compound IQOL computed by the B3LYP/6-311G (d,p) method.

Figure 5 shows a graphic depiction HOMO/LUMO Properties. The global reactivity indices for IQOL were computed, as presented in

Table 5. The calculated homo-lumo energy difference gap for IQOL is -4.32 eV, indicating higher chemical reactivity and a lower HOMO-LUMO energy gap. The HOMO donates electrons, whereas the LUMO accepts electrons. IQOL exhibits an electrophile nature of 3.403 and nucleophile range -4.215 eV. The evaluation of the chemical description parameter (GCRD) keys suggests that IQOL has strong electrophilic and nucleophilic properties. As expected, chemical hardness / softness is 2.284 and 1.143 eV, showing that the molecule is chemically stable and has sufficient strength.

The GCRD parameters revealed a much lower molecular value IQOL, the presence of a hydroxy group on the amine with a functional substituent. These characteristics in 3D graphs are demonstrated in Figure 5. The graphic shows that orbitals are largely found on HOMO and LUMO in indoloquinoline and its substituted systems. The Eg - gap energy, as seen in this Figure, means that the chemical effectively behaviour electrons, which favours the situation biological activity of compound.

Table 5. GCRD at IQOL in eV

ELUMO	- 1.70
EHOMO	- 6.02
EHOMO - ELUMO (Eg)	- 4.32
ELUMO +1	- 0.93
E HOMO-1	- 6.14
E HOMO-1 - E LUMO +1	- 5.21
Reactivity descriptors	
Electron affinity A	1.96
Ionization potential I	6.47
Chemical hardness η	2.16
Chemical softness χ	1.08
electronic chemical potential μ	- 3.86
Electronegativity χ	3.86
global electrophilicity ω	3.4467
Maximum charge transfer index D N Max	1.7870

DOS analysis

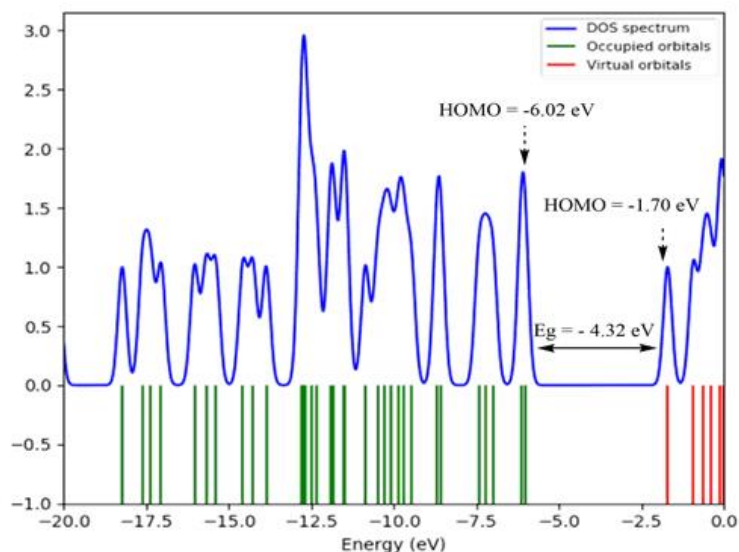


Figure 6. DOS spectrum of IQOL.

The (DOS) density of states spectrum, offers information on the amount of energy every unit of energy increment and their composition. The red and green bars on this chart show the energy values of the HOMO and LUMO, respectively. The energy of the HOMO orbital is - 6.02 eV, whereas LUMO orbital is around -1.70 eV. The energy gap E_g between the HOMO-LUMO, has been determined to - 4.32 eV. This low energy indicates allows electron movement within the indoloquinoline molecule, which is consistent with DOS spectrum measurements, as illustrated in [Figure 6](#).

DOS intensity of 0 means that the system is not observed in any condition. The transfer of electrons between C=C and C-C in the molecule's ring creates a deviation in the peak at a given energy from its original value. The lines from -20 eV to -0 eV at the beginning of the energy axis of the [Figure 6](#) are dubbed "filled orbitals", while

the lines from -5 eV to 0 eV are considered "virtual orbitals". The vacant virtual orbitals are also known as "acceptor orbitals", whereas the full orbitals are known as 'donor orbitals'. A high-intensity DOS at a given energy level implies that there are several states accessible for occupancy.

Molecular electrostatic potential surface

The MEP gives an extensive understanding of characteristics and interactions between intermolecular connections, making it an effective analysis for detecting electrophilic and nucleophilic locations in a molecular system. MEP emphasizes electrophilic locations, which have more attractive interactions, whereas nucleophilic locations suggest of significant repulsion. The opposing polar and nonpolar portions are graphically portrayed using different colors as in [Figure 7](#).

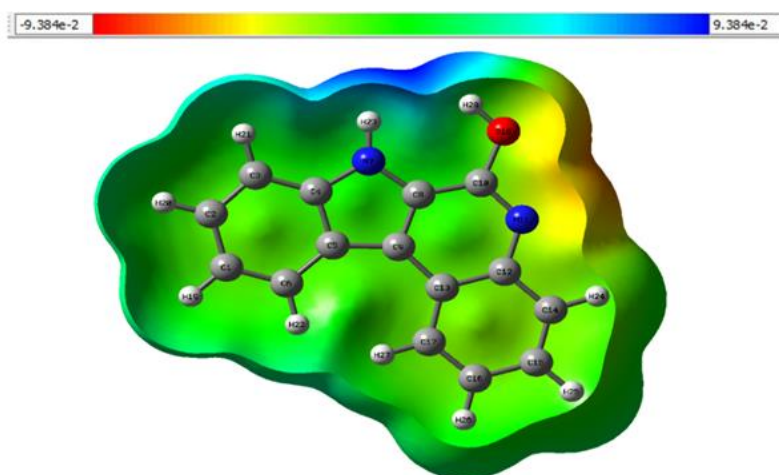


Figure 7. MEP phase for the synthesized compound IQOL.

In this representation, blue represents parts of the molecule with positive electrostatic potential values, whereas red denotes electrophilic reactivity (the most negative areas). Green and grey represent intermediate potential values between the extremes of red and dark blue. Yellow and light blue shading fill the space between the middle colour (green) and the extremes (red/dark blue). As a result, the MEP surfaces vary across the molecule from -9.384×10^{-2} (a.u.) atomic units (shown in darkest red) to 9.384×10^{-2} (a.u.) atomic units (shown in deepest blue), across the molecule.

Molecular docking studies

Molecular docking was a computational for evaluation the binding interactions between chemicals (ligands) and specific target proteins, notably those linked with COVID-19 key proteins such as 6LU7. The crystallographic data for COVID-19's major protease (Mpro) in association with the inhibitor N3 has been submitted in the Protein Data Bank (PDB) under the code 6LU7. This dataset provides essential insights into the complicated interplay between the SARS-CoV-2 virus's primary protease and the N3 inhibitor, as shown by X-ray crystallography. Oregon Health and Science University had a key role in

developing the first COVID-19 medication, chloroquine. In molecular docking, the potential activity of the synthesised molecule IQOL was investigated by docking it into the COVID-19 site. This molecular docking technique involves testing the ligand against severe acute respiratory syndrome coronavirus 2, which is represented by PDB entries like 6LU7, to distinguish and comprehend the interactions between the ligand and the related protein.

The docking technique used the AutoDock Vina approach, which involved redocking the ligand to the active site of the target COVID-19 major protein (6LU7) for validation. The alignment of the best posture of the chloroquine reference in the active site, as well as docked structures from crystallographic ligands, indicated interactions with 6LU 7. The interactions involved four typical hydrogen bonds with the Cys145, Gln189, Thr190, and Gln166 residues, with lengths of 3.52359, 2.26388, 3.5146, and 3.49926 Å, respectively. The molecule had a Pi-Pi T-shaped hydrophobic contact with His41 (bond length: 5.49112 Å) and three hydrophobic nature pi-alkyl with His163, Pro168, and Cys145 interactions (bond lengths: 3.88 to 5.46 Å) (Figure. 8).

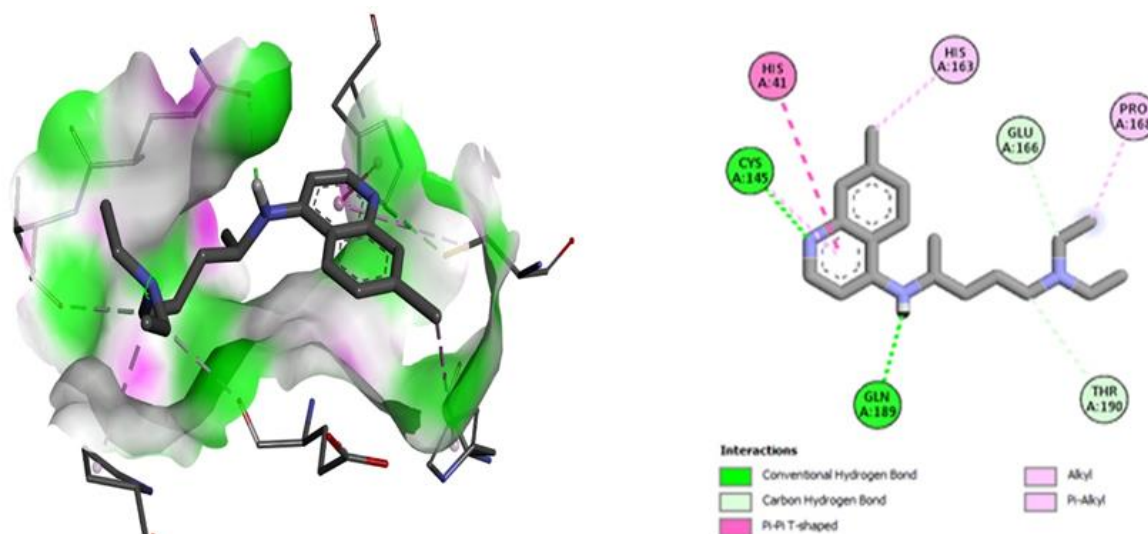


Figure 8. 2D interaction with the ligand chloroquinoline (reference): the binding site for the COVID-19 protein. PDB ID: 6LU7.

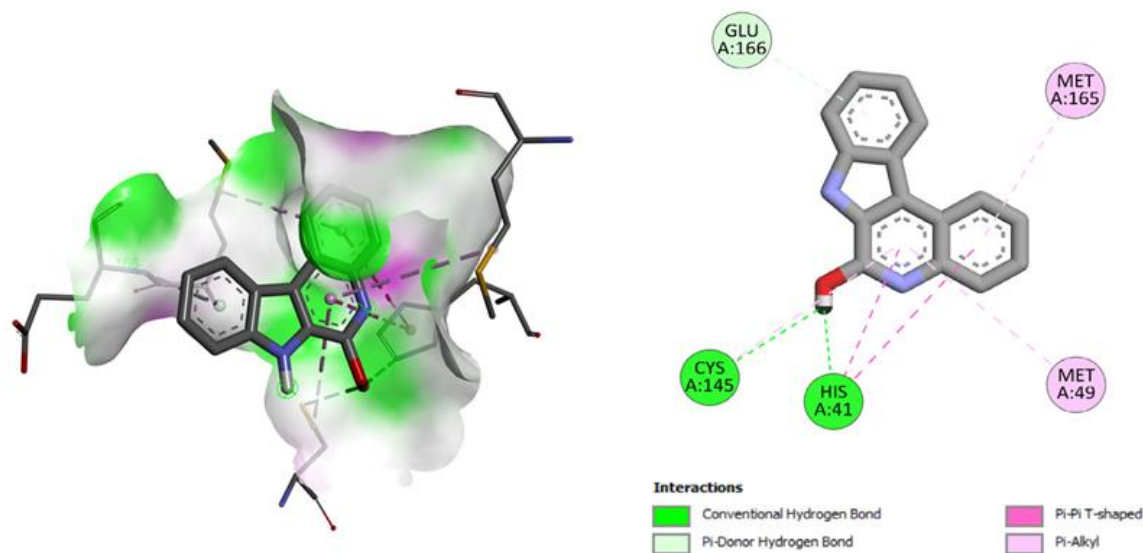


Figure 9. The docking positions of IQOL PDB ID: 6LU7.

The title compounds have low and negative binding energies, indicating a strong attraction for against COVID-19 protein. IQOL interacts with 6LU7 through three conventional hydrogen bonds interactions with Gln66, Lys145, and His41 (bond lengths: 3.898, 2.9119, 2.5666 Å), as well as two hydrophobic natures with T-shaped interactions of pi-pi bonds with His41 (bond lengths: 4.92 and 4.56 Å). There were three hydrophobic nature pi-alkyl bonds interactions found with Met165, Cys145, and Met49 (bond

lengths: 4.87, 5.46, and 4.879 Å). The discovered interaction residues facilitate the complexation of the IQOL at the active of 6LU7 (Figure. 9).

Pharmacology

ADME/Tox analysis

ADME to critical pharmacokinetic characteristics used to determine pharmacological efficacy and safety. Each component of the ADME is significant for drug

assessment. In the field of pharmacokinetics and drug similarity profiling, in-silico predictions are critical, as provided in Table 6. To evaluate a chemical compound's drug-like qualities, use Lipinski's rule of five (RO5), a set of criteria. These principles are often used in drug research and development to predict the likelihood of a molecule being an orally active medication in humans. Virtual screening techniques evaluate several factors. An oral drug must come across certain conditions, such as a molecular weight of less than 500 g/mol, equal to or fewer than 5 hydrogen bond donors (typically represented by OH or NH groups), equal to or fewer than 10 hydrogen bond acceptors (typically represented

by O or N atoms), and a Log P (octanol-water partition coefficient) value of less than 5. It is critical to understand that following Lipinski's Rule of Five does not ensure a compounds success as a medicine; rather, it serves as a guideline for finding compounds with the potential for better oral bioavailability and a higher possibility of success in drug development. Table 6 illustrates the compound for targeting COVID-19 proteins (Figure 10).

The Tox profile, developed using artificial silico approaches, has emerged as significant analysis for anticipating the pharmacologic and toxicologic features of drug applicants, mainly in the preclinical phases (Figure 11).

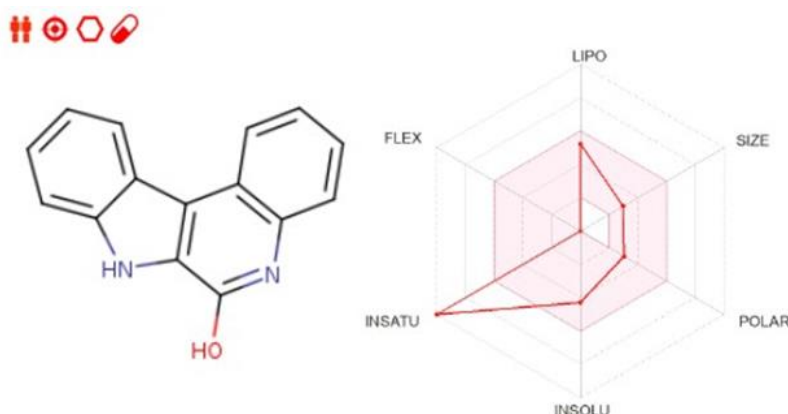


Figure 10. Bioavailability radar models of IQOL.

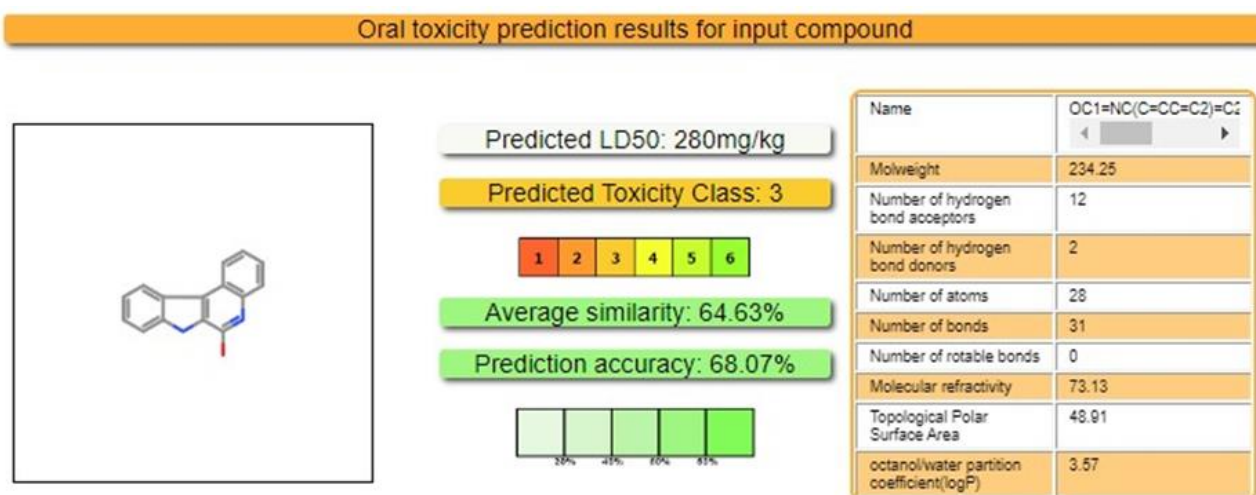


Figure 11. The *in silico* Tox profile of IQOL.

Table 6. ADME parameters^a

M.W g/mol	R B	H - A	H - D	TPSA Å ²	MR	Wlog P	ESOL log S	BBB Permeant	Log Kp cm ^s ₋₁	Lipinski Violations	PAINSalerts	GI absorption	Synthetic Accessibility
253.3 0	1	3	1	67.0 0 Å ²	72.2 4	1.90	- 4.28	Yes	- 5.15	0	0	High	1.92

^a*aR* = Rotatable bond, *H-A* = Hydrogen bond acceptor, *H-D* = hydrogen bond donor, *TPSA* = topological polar surface area, *BBB* = blood brain barrier, *log P* = lipophilicity, *log S* = water solubility, *log Kp* = permeability coefficient, and *PAINS* = pain assay interference structure.

BOILED-egg diagram

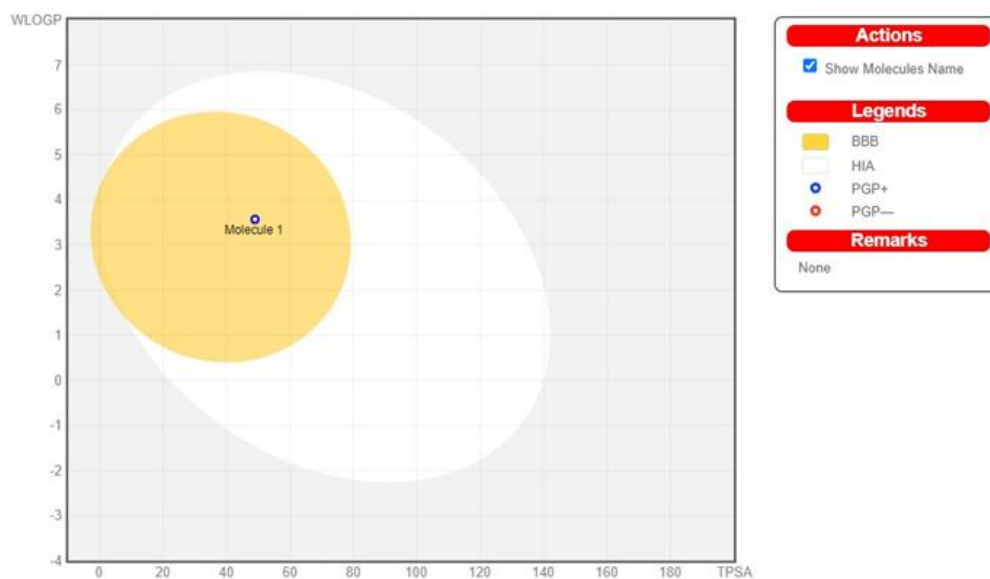


Figure 12. BOILED-Egg models of IQOL.

The study of BOILED-egg (Figure 12) shows the chemical concentration in the permitted limit for conventional medications. A bullet point with yellow region signifies that the drug remains unaffected by the CNS P-glycoprotein, whereas a blue dot in the cooked egg graphic indicates passive penetration of the blood-brain barrier. The red zone represents the capacity to persist in the brain. The synthesised ligand and its complexes satisfied the required requirements, indicating high bioavailability. These findings demonstrate that the chemical is safe and unlikely to induce skin allergies. Interestingly, the drug ratings for these substances were modest.

Conclusion

A simple and effective technique for synthesizing derivatives of IQOL, attaining exceptionally high yields via a two-step process. The synthesised compounds were thoroughly characterized using FT-IR, ¹H, ¹³C-NMR, and GC-MS. Further travelled using DFT calculations, which revealed outstanding agreement between the expected robustness of our theoretical predictions and experimental results. Molecular docking tests demonstrated significant between the title compound and the target protein (6LU7), indicating ADME/Tox these findings highlight the possibility of these indoloquinoline

(IQOL) as attractive applicants for the development of novel COVID-19.

Conflict of interest

The authors have no conflict of interest in this study.

Orcid

M. Vijayarathinam : 0009-0000-3042-2608

A. Kannan : 0009-0003-7986-4003

P. Akilan : 0009-0000-8131-3524

T. Gunasekaran : 0009-0006-5125-4918

References

- [1] C. Challa, J. Ravindran, M.M. Konai, S. Varughese, J. Jacob, B.D. Kumar, J. Haldar, R.S. Lankalapalli, Expedient synthesis of indolo [2, 3-*b*] quinolines, chromeno [2, 3-*b*] indoles, and 3-alkenyl-oxindoles from 3, 3'-diindolylmethanes and evaluation of their antibiotic activity against methicillin-resistant *Staphylococcus aureus*, *ACS Omega*, **2017**, 2, 5187-5195. [[Crossref](#)], [[Google Scholar](#)], [[Publisher](#)]
- [2] P. Pitchai, M. Sathiyaseelan, A. Nepolraj, R. Gengan, An elegant synthesis of indoloquinoline alkaloid cryptotackieine via Vilsmeier-Haack approach, *Indian Journal of Chemistry*, **2015**, 54, 1290-1292. [[Google Scholar](#)]
- [3] A.M. Psaras, R.K. Carty, J.T. Miller, L.N. Tumey, T.A. Brooks, Indoloquinoline-Mediated Targeted Downregulation of KRAS through Selective Stabilization of the Mid-Promoter G-Quadruplex Structure, *Genes*, **2022**, 13, 1440. [[Crossref](#)], [[Google Scholar](#)], [[Publisher](#)]
- [4] C.K. Tudu, A. Bandyopadhyay, M. Kumar, Radha, T. Das, S. Nandy, M. Ghorai, A.V. Gopalakrishnan, J. Proćków, A. Dey, Unravelling the pharmacological properties of cryptolepine and its derivatives: a mini-review insight, *Naunyn-schmiedeberg's Archives of Pharmacology*, **2023**, 396, 229-238. [[Crossref](#)], [[Google Scholar](#)], [[Publisher](#)]
- [5] M. Shiri, M.M. Heravi, H. Hamidi, M.A. Zolfigol, Z. Tanbakouchian, A. Nejatinezhad-Arani, S.A. Shintre, N.A. Koorbanally, Transition metal-free synthesis of quinolino [2', 3': 3, 4] pyrazolo [5, 1-*b*] quinazolin-8 (6 *H*)-ones via cascade dehydrogenation and intramolecular *N*-arylation, *Journal of the Iranian Chemical Society*, **2016**, 13, 2239-2246. [[Crossref](#)], [[Google Scholar](#)], [[Publisher](#)]
- [6] Y.M. Vianney, K. Weisz, Indoloquinoline Ligands Favor Intercalation at Quadruplex-Duplex Interfaces, *Chemistry–A European Journal*, **2022**, 28, e202103718. [[Crossref](#)], [[Google Scholar](#)], [[Publisher](#)]
- [7] M.O. Aggrey, W.Q. Wang, L.J. Xuan, Novel indoloquinoline alkaloid glycosides from *Cryptolepis sanguinolenta* (Lindl.) Schltr, *Natural Product Research*, **2023**, 1-7. [[Crossref](#)], [[Google Scholar](#)], [[Publisher](#)]
- [8] S.O. Bekoe, E. Orman, S.A. Adjabui, A.A. Brobbey, J. Oppong-Kyekyeku, K.F.-M. Opuni, N. Kuntworbe, S. Asare-Nkansah, Development and validation of an ion-pair HPLC-UV method for the quantitation of quinoline and indoloquinoline alkaloids in herbal and pharmaceutical antimalarial formulations, *Journal of Chemistry*, **2022**, 2022. [[Crossref](#)], [[Google Scholar](#)], [[Publisher](#)]
- [9] A. Paulo, E.T. Gomes, J. Steele, D.C. Warhurst, P.J. Houghton, Antiplasmodial activity of *Cryptolepis sanguinolenta* alkaloids from leaves and roots, *Planta Medica*, **2000**, 66, 30-34. [[Crossref](#)], [[Google Scholar](#)], [[Publisher](#)]
- [10] C. Bailly, W. Laine, B. Baldeyrou, D. Pauw-Gillet, P. Colson, C. Houssier, K. Cimanga, S. Van Miert, A.J. Vlietinck, L. Pieters, DNA intercalation, topoisomerase II inhibition and cytotoxic activity of the plant alkaloid neocryptolepine, *Anti-cancer Drug Design*, **2000**, 15, 191-201. [[Google Scholar](#)], [[Publisher](#)]

- [11] H. Hamidi, M.M. Heravi, M. Tajbakhsh, M. Shiri, H.A. Oskooie, S.A. Shintre, N.A. Koorbanally, Synthesis and anti-bacterial evaluation of novel thio-and oxazepino [7, 6-b] quinolines, *Journal of the Iranian Chemical Society*, **2015**, *12*, 2205-2212. [[Crossref](#)], [[Google Scholar](#)], [[Publisher](#)]
- [12] A. Nepolraj, P. Pitchai, M. Vijayarathinam, A Facile Synthesis of 2-Hydroxy-3-Phenylquinoline Derivatives, *Malaysian Journal of Chemistry*, **2019**, *21*, 66. [[Google Scholar](#)], [[PDF](#)]
- [13] S. Manisekar, S. Kannadasan, N. Amaladoss, S. Vasyil, Design, Synthesis and Molecular Docking Studies of Indolo [2, 3-a] Acridinol Derivatives, *Макрогетероциклы*, **2022**, *15*, 59-66. [[Crossref](#)], [[Google Scholar](#)], [[Publisher](#)]
- [14] V.I. Shupeniuk, A. Nepolraj, T.N. Taras, O.P. Sabadakh, M.P. Matkivskyi, Y.R. Luchkevych, In-silico study of anthraquinone derivatives as probable inhibitors of COVID-19, *Journal of Chemistry and Technologies*, **2022**, *30*, 151-158. [[Google Scholar](#)]
- [15] A.A. Alkathiri, A. Atta, M.S. Refat, S. Shakya, A. Hassanien, S.A. Algarni, E.M. Ahmed, S.E. Alomariy, M. Alsawat, N. Algethami, Impedance spectroscopy and DFT/TD-DFT studies of diyttrium trioxide for optoelectronic fields, *Journal of Rare Earths*, **2023**, *41*, 605-612. [[Crossref](#)], [[Google Scholar](#)], [[Publisher](#)]
- [16] N.E. Kirchner-Hall, W. Zhao, Y. Xiong, I. Timrov, I. Dabo, Extensive benchmarking of DFT+ U calculations for predicting band gaps, *Applied Sciences*, **2021**, *11*, 2395. [[Crossref](#)], [[Google Scholar](#)], [[Publisher](#)]
- [17] M. Muniz-Miranda, F. Muniz-Miranda, M.C. Menziani, A. Pedone, Can DFT Calculations Provide Useful Information for SERS Applications?, *Molecules*, **2023**, *28*, 573. [[Crossref](#)], [[Google Scholar](#)], [[Publisher](#)]
- [18] M. Bursch, J.M. Mewes, A. Hansen, S. Grimme, Best-practice DFT protocols for basic molecular computational chemistry, *Angewandte Chemie International Edition*, **2022**, *61*, e202205735. [[Crossref](#)], [[Google Scholar](#)], [[Publisher](#)]
- [19] J. Singh, M.S. Khan, S. Uddin, A DFT study of vibrational spectra of 5-chlorouracil with molecular structure, HOMO-LUMO, MEPs/ESPs and thermodynamic properties, *Polymer Bulletin*, **2023**, *80*, 3055-3083. [[Crossref](#)], [[Google Scholar](#)], [[Publisher](#)]
- [20] M. Drissi, N. Benhalima, Y. Megrouss, R. Rachida, A. Chouaih, F. Hamzaoui, Theoretical and experimental electrostatic potential around the m-nitrophenol molecule, *Molecules*, **2015**, *20*, 4042-4054. [[Crossref](#)], [[Google Scholar](#)], [[Publisher](#)]
- [21] D. Mishra, R.R. Maurya, K. Kumar, N.S. Munjal, V. Bahadur, S. Sharma, P. Singh, I. Bahadur, Structurally modified compounds of hydroxychloroquine, remdesivir and tetrahydrocannabinol against main protease of SARS-CoV-2, a possible hope for COVID-19: Docking and molecular dynamics simulation studies, *Journal of Molecular Liquids*, **2021**, *335*, 116185. [[Crossref](#)], [[Google Scholar](#)], [[Publisher](#)]
- [22] S.J.Y. Macalino, V. Gosu, S. Hong, S. Choi, Role of computer-aided drug design in modern drug discovery, *Archives of pharmacal research*, **2015**, *38*, 1686-1701. [[Crossref](#)], [[Google Scholar](#)], [[Publisher](#)]
- [23] C.M. Song, S.J. Lim, J.C. Tong, Recent advances in computer-aided drug design, *Briefings in Bioinformatics*, **2009**, *10*, 579-591. [[Crossref](#)], [[Google Scholar](#)], [[Publisher](#)]
- [24] W. Lu, R. Zhang, H. Jiang, H. Zhang, C. Luo, Computer-aided drug design in epigenetics, *Frontiers in Chemistry*, **2018**, *6*, 57. [[Crossref](#)], [[Google Scholar](#)], [[Publisher](#)]
- [25] C.S. Odoemelam, E. Hunter, J. Simms, Z. Ahmad, M.W. Chang, B. Percival, I.H. Williams, M. Molinari, S.C.L. Kamerlin, P.B. Wilson, In silico ligand docking approaches to characterise the binding of known allosteric

- modulators to the glucagon-like peptide 1 receptor and prediction of ADME/Tox properties, *Applied Biosciences*, **2022**, *1*, 143-162. [[Crossref](#)], [[Google Scholar](#)], [[Publisher](#)]
- [26] H. Yu, A. Adedoyin, ADME-Tox in drug discovery: integration of experimental and computational technologies, *Drug Discovery Today*, **2003**, *8*, 852-861. [[Crossref](#)], [[Google Scholar](#)], [[Publisher](#)]
- [27] N.A. Durán-Iturbide, B.I. Díaz-Eufracio, J.L. Medina-Franco, In silico ADME/Tox profiling of natural products: A focus on BIOFACQUIM, *ACS Omega*, **2020**, *5*, 16076-16084. [[Crossref](#)], [[Google Scholar](#)], [[Publisher](#)]
- [28] D. Yang, Y. Zhou, N. Xue, J. Qu, Synthesis of trifluoromethyl ketones via tandem claisen condensation and retro-claisen C-C bond-cleavage reaction, *The Journal of Organic Chemistry*, **2013**, *78*, 4171-4176. [[Crossref](#)], [[Google Scholar](#)], [[Publisher](#)]
- [29] M.S. Kirillova, M.E. Muratore, R. Dorel, A.M. Echavarren, Concise total synthesis of lundurines A-C enabled by gold catalysis and a homodienyl retro-ene/ene isomerization, *Journal of the American Chemical Society*, **2016**, *138*, 3671-3674. [[Crossref](#)], [[Google Scholar](#)], [[Publisher](#)]
- [30] J.L. Vique-Sánchez, Potential inhibitors interacting in Neuropilin-1 to develop an adjuvant drug against COVID-19, by molecular docking, *Bioorganic & Medicinal Chemistry*, **2021**, *33*, 116040. [[Crossref](#)], [[Google Scholar](#)], [[Publisher](#)]
- [31] A. Bag, A. Bag, Treatment of COVID-19 patients: Justicia adhatoda leaves extract is a strong remedy for COVID-19-Case report analysis and docking based study, **2020**. [[Google Scholar](#)], [[Publisher](#)]
- [32] R. Kong, G. Yang, R. Xue, M. Liu, F. Wang, J. Hu, X. Guo, S. Chang, COVID-19 Docking Server: A meta server for docking small molecules, peptides and antibodies against potential targets of COVID-19, *Bioinformatics*, **2020**, *36*, 5109-5111. [[Crossref](#)], [[Google Scholar](#)], [[Publisher](#)]
- [33] B.L. Zhong, W. Luo, H.M. Li, Q.Q. Zhang, X.G. Liu, W.T. Li, Y. Li, Knowledge, attitudes, and practices towards COVID-19 among Chinese residents during the rapid rise period of the COVID-19 outbreak: a quick online cross-sectional survey, *International Journal of Biological Sciences*, **2020**, *16*, 1745. [[Crossref](#)], [[Google Scholar](#)], [[Publisher](#)]
- [34] M. Yıldırım, Ö. Akgül, E. Geçer, The effect of COVID-19 anxiety on general health: The role of COVID-19 coping, *International journal of Mental Health and Addiction*, **2022**, *20*, 1110-1121. [[Crossref](#)], [[Google Scholar](#)], [[Publisher](#)]
- [35] Y.C. Wu, C.S. Chen, Y.J. Chan, The outbreak of COVID-19: An overview, *Journal of the Chinese Medical Association*, **2020**, *83*, 217-220. [[Crossref](#)], [[Google Scholar](#)], [[Publisher](#)]
- [36] B. Hu, S. Huang, L. Yin, The cytokine storm and COVID-19, *Journal of Medical Virology*, **2021**, *93*, 250-256. [[Crossref](#)], [[Google Scholar](#)], [[Publisher](#)]
- [37] D.K. Ahorsu, C.Y. Lin, V. Imani, M. Saffari, M.D. Griffiths, A.H. Pakpour, The fear of COVID-19 scale: Development and initial validation, *International Journal of Mental Health and Addiction*, **2020**, 1-9. [[Crossref](#)], [[Google Scholar](#)], [[Publisher](#)]
- [38] P. Jayavel, V. Ramasamy, N. Amaladoss, V. Renganathan, V.I. Shupeniuk, A facile synthesis, characterization, DFT, ADMET and in-silico molecular docking analysis of novel 4-ethyl acridine-1, 3, 9 (2, 4, 10*H*)-trione, *Chemical Physics Impact*, **2024**, *8*, 100476. [[Crossref](#)], [[Google Scholar](#)], [[Publisher](#)]
- [39] S. Sajjadifar, K. Pal, H. Jabbari, O. Pournalimardan, F. Divsar, S. Mohammadi-Aghdam, I. Amini, H. Hamidi, Characterization of catalyst: comparison of Brønsted and Lewis acidic power in boron sulfonic acid as a heterogeneous catalyst in green synthesis of quinoxaline derivatives, *Chemical*

- Methodologies*, **2019**, *3*, 145-275. [[Crossref](#)], [[Google Scholar](#)], [[Publisher](#)]
- [40] M. Dai, K. Khan, S. Zhang, K. Jiang, X. Zhang, W. Wang, L. Liang, H. Cao, P. Wang, P. Wang, A direct method to extract transient sub-gap density of state (DOS) based on dual gate pulse spectroscopy, *Scientific Reports*, **2016**, *6*, 24096. [[Crossref](#)], [[Google Scholar](#)], [[Publisher](#)]
- [41] W. Chen, W. Wu, L. Zhou, M. Xu, L. Wang, H. Ning, J. Peng, A semi-analytical extraction method for interface and bulk density of states in metal oxide thin-film transistors, *Materials*, **2018**, *11*, 416. [[Crossref](#)], [[Google Scholar](#)], [[Publisher](#)]
- [42] C. Cassidy, J. Halbout, W. Donaldson, C. Tang, Nonlinear optical properties of urea, *Optics Communications*, **1979**, *29*, 243-246. [[Crossref](#)], [[Google Scholar](#)], [[Publisher](#)]

HOW TO CITE THIS ARTICLE

M. Vijayarathinam, A. Kannan, P. Akilan, V. Chandrasekaran, T. Gunasekaran. A Novel Approach in the Synthesis of Indoloquinoline Alkaloid Analogues: Spectroscopic and DFT Exploration, Molecular Docking of COVID-19, and ADMET Properties. *Adv. J. Chem. A*, 2024, 7(4), 417-437.

DOI: [10.48309/AJCA.2024.437859.1484](https://doi.org/10.48309/AJCA.2024.437859.1484)

URL: https://www.ajchem-a.com/article_193266.html